

REGULAR PAPERS

Transport characteristics of minority electrons across surface-activated-bonding based p-Si/n-4H-SiC heterointerfaces

To cite this article: Naoteru Shigekawa *et al* 2018 *Jpn. J. Appl. Phys.* **57** 02BE04

View the [article online](#) for updates and enhancements.



Transport characteristics of minority electrons across surface-activated-bonding based p-Si/n-4H-SiC heterointerfaces

Naoteru Shigekawa^{1*}, Sae Shimizu¹, Jianbo Liang¹, Masato Shingo², Kenji Shiojima², and Manabu Arai³

¹Graduate School of Engineering, Osaka City University, Osaka 558-8585, Japan

²Graduate School of Electrical and Electronics Engineering, University of Fukui, Fukui 910-8507, Japan

³New Japan Radio Co., Ltd., Fujimino, Saitama 356-8510, Japan

*E-mail: shigekawa@elec.eng.osaka-cu.ac.jp

Received June 18, 2017; revised October 15, 2017; accepted October 18, 2017; published online January 15, 2018

We investigate the transport properties of minority electrons across p-Si/n-4H-SiC interfaces fabricated using surface activated bonding. The transport properties along each direction are examined by measuring the photoresponse (PR) of p-Si/n-4H-SiC heterojunctions and characterizing 4H-SiC/Si heterojunction bipolar transistors (HBTs). The photoyield obtained in PR measurements is sensitive to the concentration of acceptors in p-Si and reverse-bias voltages, which indicates that the energy of optically excited electrons in p-Si is first relaxed and then they are driven to n-SiC through the tunneling process. By the postprocess annealing of HBTs, the properties of emitter/base interfaces are improved so that the current gain is drastically increased, which means that the Si/4H-SiC interfaces are in metastable states when the device process is completed. A maximum current gain of >10 is demonstrated. © 2018 The Japan Society of Applied Physics

1. Introduction

Semiconductor heterojunctions made of narrow-gap and wide-gap materials are ideal systems for electron devices that handle high powers at high frequencies because both of the advantages of the respective materials—the excellent transport properties of narrow-gap semiconductors^{1,2)} and the high breakdown characteristics of wide gap semiconductors^{3,4)}—can be utilized in single devices by optimizing their potential profiles. However, we find difficulties in fabricating such heterojunctions using epitaxial growth technologies since there are large differences in lattice constants and thermal expansion coefficients between typical narrow-gap semiconductors, such as GaAs, Si, and Ge, and wide-gap semiconductors such as GaN and 4H-SiC,⁵⁾ although Si/3C-SiC,⁶⁾ Si/4H-SiC,⁷⁾ and GaAs/GaN junctions⁸⁾ have been epitaxially grown in pioneering works.

Wafer bonding technologies^{5,9)} such as surface activated bonding (SAB)¹⁰⁾ provide a practical solution to overcoming such difficulties. Several authors reported on wafer-bonding-based GaAs/GaN,¹¹⁾ GaAs/4H-SiC,^{12,13)} and Si/4H-SiC junctions.^{14–17)} We previously fabricated Si/4H-SiC pn and nn junctions by SAB, and found that ≈6-nm-thick amorphous-like layers observed at the as-bonded Si/SiC interfaces were recrystallized and the reverse-bias characteristics as well as the ideality factors were improved when the junctions were annealed at 1000 °C for 60 s in N₂ ambient.^{18,19)} By using the scanning internal photoemission microscopy technique,²⁰⁾ the correlation between the spatially resolved photoyield, which is defined as the photocurrent normalized by the number of incident photons per second, and the structures of Si/SiC interfaces were investigated.²¹⁾ Recently, we have briefly discussed the threshold energy in the photoresponse (PR) of Si/4H-SiC pn junctions as well as the room-temperature properties of 4H-SiC/Si heterojunction bipolar transistors,²²⁾ in which the emitter, base, and collector were made of n-4H-SiC, p-Si, and n-Si, respectively.²³⁾

In this study, we intensively investigate the PR of the Si/4H-SiC pn junctions and the electrical characteristics of the 4H-SiC/Si heterojunction bipolar transistors (HBTs). The effects of the impurity concentration in p-Si layers and the

reverse-bias voltages are focused on in the discussion of PR. The impacts of the postprocess annealing are highlighted in the characterization of the HBTs. Using these two approaches, the transport properties of the minority electrons along each direction across the bonding interfaces, i.e., (i) the minority electrons that are optically excited in the p-Si layer and driven toward the n-4H-SiC layer and (ii) those that are electrically injected from the n-4H-SiC layer to the p-Si layer, are examined. It is noteworthy that the transport characteristics of the minority carriers are more sensitive to the properties of interfaces in comparison with the transport characteristics of the majority carriers.

2. Methods

2.1 Sample fabrication and diagram for photoresponse measurement

We prepared an n⁻-SiC epitaxial layer (donor concentration $N_D = 5.4 \times 10^{15} \text{ cm}^{-3}$, 10 μm) on an n⁺-4H-SiC (0001) substrate via an n-SiC buffer layer ($N_D = 1 \times 10^{18} \text{ cm}^{-3}$, 0.5 μm). The 4H-SiC substrate has an off-angle of 4° toward the [11 $\bar{2}$ 0] direction. Using SAB facilities equipped with fast atom beam (FAB) guns of Ar, the SiC epitaxial layer was bonded to each of two B-doped p-Si(100) substrates with different acceptor concentrations ($N_A = 2.4 \times 10^{17}$ and $2.6 \times 10^{19} \text{ cm}^{-3}$). The acceleration voltage and duration of FAB irradiation were ~2 kV and 180 s, respectively. The substrates were pressed to each other with a force of ~10 MPa for 60 s to fabricate the junctions. The substrates were not heated during the bonding. By forming ohmic contacts on the back surfaces of the SiC and Si substrates and dicing, two types of Si/SiC pn junctions were prepared. The pn junctions made of the lightly and heavily doped p-Si substrates are hereafter referred to as (A) and (B), respectively. A monochromatic light with a photon energy $h\nu$ in the range between 1.38 and 4 eV was focused on the part of the back surface of the SiC substrate that was not masked by the ohmic contacts. We then measured the photoyield (Y) of the pn junctions. A schematic cross section of the fabricated pn junctions as well as the configuration of measurements are shown in Fig. 1.

2.2 C-up HBT fabrication

We fabricated collector-up (C-up) 4H-SiC/Si HBTs using the

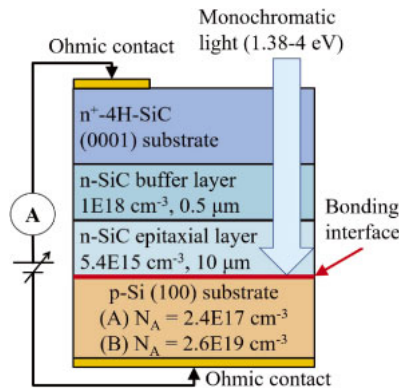


Fig. 1. (Color online) Schematic cross section of pn junctions employed in the photoresponse measurements as well as the configuration of measurements.

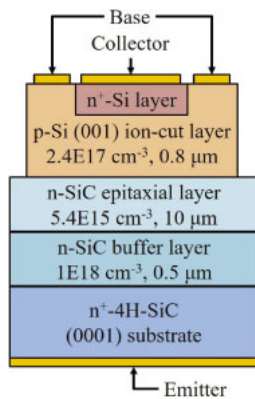


Fig. 2. (Color online) Schematic cross section of C-up HBTs.

process sequences of (i) bonding of an n^- -SiC epitaxial layer grown on an n -4H-SiC (0001) substrate and a p-Si(001) substrate, (ii) fabricating a ≈ 800 -nm-thick $400 \times 500 \mu\text{m}^2$ Si mesa by the ion-cut process and mesa etching, (iii) defining a $300\text{-}\mu\text{m}$ - ϕ circular collector region on the Si mesa by P ion implantation, (iv) evaporating an emitter contact metal layer on the back surface of the SiC substrate, (v) annealing at 700°C for 10 min to produce the emitter contact, activate the implanted P atoms, and improve the properties of the bonding interfaces, and (vi) forming base contacts by evaporating a contact metal layer (Al/Ni/Au) and annealing at 400°C for 1 min. The SiC epitaxial layer and p-Si substrate employed were the same as those used for fabricating (A) for PR measurements. The conditions for the bonding process were the same as those for fabricating pn junctions for PR measurements. The areas of base mesas, base contacts, and collector contacts are 2×10^{-3} , 1×10^{-3} , and $7 \times 10^{-4} \text{cm}^2$, respectively. A schematic cross section of HBTs is shown in Fig. 2.

We additionally annealed HBT dies at 400 and 700°C for 1 min after the above process sequence was completed (postprocess annealing). All of the annealing steps were carried out in N_2 ambient. The characteristics of the dies were measured at room temperature.

3. Results and discussion

3.1 Photoresponse of Si/SiC pn heterointerfaces

The square root of the photoyield (\sqrt{Y}) of (A) without bias voltages is shown in Fig. 3(a). Its lower-energy ($h\nu < 1.8 \text{eV}$)

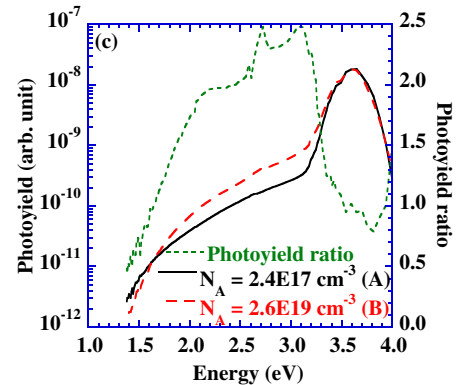
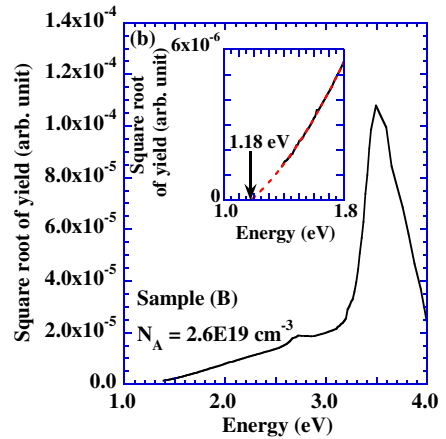
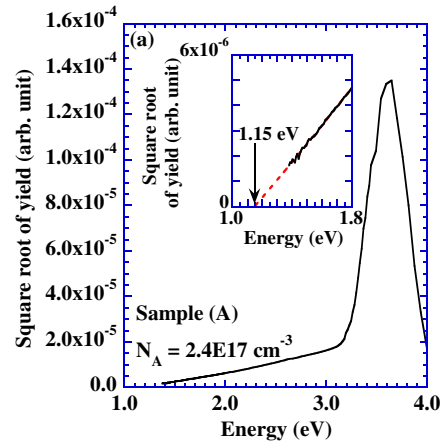


Fig. 3. (Color online) Square root of the photoyield of (a) unbiased Sample (A) with $N_A = 2.4 \times 10^{17} \text{cm}^{-3}$ and (b) unbiased Sample (B) with $N_A = 2.6 \times 10^{19} \text{cm}^{-3}$. (c) Photoyield spectra of unbiased (A) and unbiased (B) are shown. The photoyield ratio is also shown.

part is depicted in an inset at a magnified scale. A peak observed at 3.6eV was attributed to the absorption in the n -SiC layer with a bandgap of 3.24eV . \sqrt{Y} in the lower-energy part was proportional to the photon energy. \sqrt{Y} of (B) is shown in Fig. 3(b). In contrast to (A), \sqrt{Y} of (B) in the lower-energy parts revealed a slight warp. The lower-energy parts of \sqrt{Y} were fitted to a quadratic function so as to phenomenologically include the contribution of the warp. Using the fitting, the threshold energy corresponding to $\sqrt{Y} = 0$ was estimated to be ≈ 1.15 and $\approx 1.18 \text{eV}$ for (A) and (B), respectively, which were both close to the bandgap of intrinsic Si (1.12eV at room temperature). The results of fitting are shown in the insets of the respective figures. We found that uncertainties in the estimated threshold energies were ≈ 10 – 20meV .

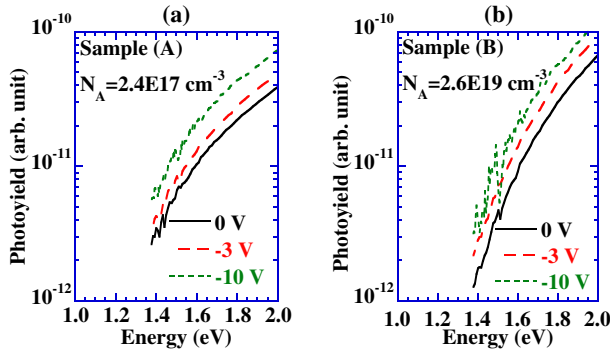


Fig. 4. (Color online) (a) Photoyield spectra of Sample (A) under 0 (unbiased), -3, and -10 V. (b) Photoyield spectra of Sample (B) under 0 (unbiased), -3, and -10 V. Negative bias voltages correspond to the reverse-bias condition.

The photoyield spectra of (A) and (B) are shown in Fig. 3(c). Their ratio, Y of (B) divided by that of (A), is also shown in this figure. The photoyield ratio increased as $h\nu$ increased from 1.4 to 2 eV. The ratio remained between 2 and 2.5 for higher photon energies up to 3.2 eV. The ratio decreased as $h\nu$ increased beyond 3.2 eV, or the contribution of the SiC layer was more pronounced. Y of (B) is smaller than that of (A) for $h\nu < 1.7$ eV. For $1.7 < h\nu < 3.2$ eV, in contrast, Y of (B) is larger than that of (A).

Y for reverse-bias voltages of -3 and -10 V as well as Y without bias voltages are shown for (A) and (B) in Figs. 4(a) and 4(b), respectively. Y was increased by applying reverse bias voltages in each sample. It was found that the separation between the respective curves, i.e., the degree of increase in Y , was almost independent of $h\nu$.

Y for $h\nu < 3.24$ eV is assumed to be attributed to the photoabsorption of the p-Si layers. Noting the indirect properties of Si, the dependence of Y on $h\nu$ in this energy range can be expressed as

$$Y \propto (h\nu - E_{G,\text{Si}})^2, \quad (1)$$

where $E_{G,\text{Si}}$ is the apparent bandgap of Si. The result that \sqrt{Y} was almost linearly dependent on $h\nu$ and the threshold energy was close to the bandgap of intrinsic Si is consistent with the above scheme. The slight warp observed for (B) [Fig. 3(b)] is likely to be attributable to the heavy doping, as previously reported for the photoabsorption of heavily B-doped ($N_A = 10^{19} \text{ cm}^{-3}$) p-Si.²⁴

The dependence of photoyield spectra on reverse-bias voltages suggest that the energy of optically excited electrons was first relaxed, then the electrons were driven toward the interfaces through the drift-diffusion process, piled up at the interfaces, and tunneled to the conduction band of the SiC layer.

The density of the minority electrons (n) inside of the p-Si layers ($x < 0$) is described using the drift-diffusion model. Using this model, the continuity condition of current due to the minority electrons is expressed as²⁵

$$\frac{\partial n}{\partial t} = \frac{I_0}{L_{\text{ph}}} \exp\left(\frac{x}{L_{\text{ph}}}\right) - \frac{n - n_0}{\tau_n} + n\mu \frac{\partial E}{\partial x} + \mu E \frac{\partial n}{\partial x} + D_n \frac{\partial^2 n}{\partial x^2}. \quad (2)$$

In this expression, I_0 is the intensity of the incident light at $x = 0$ (the interface), E is the electric field, and n_0 is the

minority electron density in the equilibrium condition. D_n , τ_n , and μ are the diffusion coefficient, lifetime, and mobility of the minority electrons, respectively. L_{ph} is the penetration depth of the incident photons into the p-Si layers.

We consider the steady-state condition ($\partial n / \partial t = 0$). In addition, given that the electric field is only apparent in a submicron region neighboring the interface (not depicted),²³ we assume that $E = 0$ in the above equation, i.e., we only consider the motion of electrons due to the diffusion. Using this crude approximation, the minority electron concentration at the interface is analytically expressed as

$$n - n_0|_{x=0} = \frac{I_0 \tau_n}{2(L_n + L_{\text{ph}})}, \quad (3)$$

where L_n stands for the diffusion length of the minority electrons in p-Si ($L_n = \sqrt{D_n \tau_n}$). The ratio of $n - n_0|_{x=0}$ in (B) to $n - n_0|_{x=0}$ in (A) is, consequently, given by

$$\frac{n - n_0|_{x=0,\text{B}}}{n - n_0|_{x=0,\text{A}}} = \frac{\tau_{n,\text{B}} L_{n,\text{A}} + L_{\text{ph}}}{\tau_{n,\text{A}} L_{n,\text{B}} + L_{\text{ph}}}. \quad (4)$$

L_n for (A) and (B) is estimated to be $L_{n,\text{A}} \approx 40 \mu\text{m}$ and $L_{n,\text{B}} \approx 2\text{--}3 \mu\text{m}$, respectively.²⁶ L_{ph} decreases from ≈ 20 to $\approx 3 \mu\text{m}$ as $h\nu$ increases from 1.4 to 2 eV.²⁷ As L_{ph} decreases ($h\nu$ increases), the ratio increases so that the photoyield of (B) becomes more apparent in comparison with that of (A). Physically, at low photon energies such as $h\nu = 1.4$ eV, the major parts of optically excited electrons are likely to recombine inside of the p-Si layer of (B) since $L_{n,\text{B}} \ll L_{\text{ph}}$. In (A), in contrast, a certain portion of electrons is assumed to reach to the SiC/Si interfaces, which explains the result that \sqrt{Y} of (B) was smaller than that of (A). As $h\nu$ increases, the penetration depth of photons decreases, so that a larger number of excited electrons are likely to arrive at the interfaces in (B). The photoyield ratio should, consequently, increase.

The electric field at the interface in (B) is likely to be higher than that in (A) because of the difference in N_A in p-Si substrates. The tunneling probability of electrons at the interface in (B) is, consequently, assumed to be larger than that in (A). The photoyield ratio of >1 in the high-energy range ($1.7 \text{ eV} < h\nu$) can be qualitatively explained by this hypothesis.

3.2 Effects of postprocess annealing on SiC/Si HBTs

Figure 5(a) shows the relationship between the collector current I_C and the collector-base voltage V_{CB} of an HBT die without annealing. The relationships in dies after postprocess annealing at 400 °C for 1 min, and 700 °C for 1 min are shown in Figs. 5(b) and 5(c), respectively. The emitter current I_E was varied between 0 and 5 mA in steps of 1 mA. The differential common-base current gains α at $V_{\text{CB}} = 0$ V were ≈ 0.09 and ≈ 0.9 after the 400 and 700 °C annealing, respectively, which was in marked contrast to the result for the die without annealing ($\alpha \sim 0.01$). We also found that the leakage across the base/collector junction was more marked in the 700 °C-annealed die than in the other two dies. The I_C of as low as 5 mA, which corresponded to the collector current density of 7 A/cm^2 , and the apparent leakage in I_C - V_{CB} characteristics are explained by the low doping concentration in the SiC emitter and the immaturity of the process for fabricating base/collector junctions, respectively.

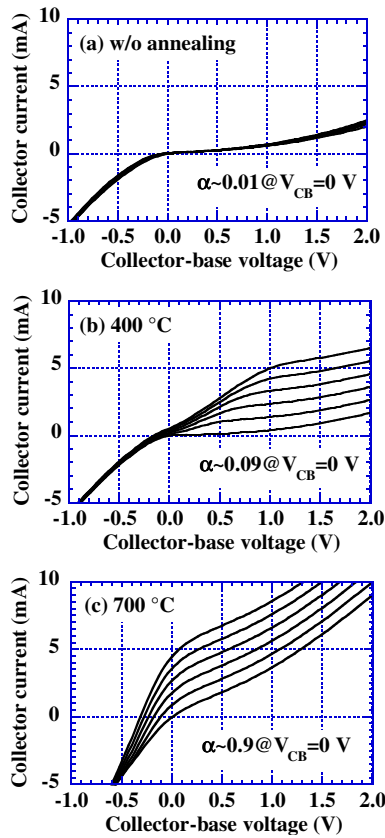


Fig. 5. (Color online) I_C - V_{CB} characteristics of 4H-SiC/Si HBT dies without annealing (a), annealed at 400 °C for 1 min (b), and at 700 °C for 1 min (c). I_E was varied between 0 and 5 mA in steps of 1 mA.

Gummel plots, or dependences of the base current I_B and I_C on the base-emitter voltage V_{BE} for $V_{CB} = 0$ V, of a die without annealing, a 400 °C-annealed die, and a 700 °C-annealed die are shown in Figs. 6(a), 6(b), and 6(c), respectively. The differential common-emitter current gain β ($\equiv dI_C/dI_B$) is also shown in each figure. The maximum of β (β_{max}) was ≈ 0.14 and ≈ 10.3 for the 400 °C- and 700 °C-annealed dies, respectively. β_{max} for the 700 °C-annealed die was ≥ 300 times as large as that for the nonannealed die (~ 0.03).

Figure 7 shows I - V characteristics for forward-bias voltages of the emitter/base diodes for the three samples. A hump observed at ≈ 0.2 V for the nonannealed die, which was attributed to the recombination at the interfaces, was not present in the characteristics of the two annealed dies. The ideality factor for both the nonannealed and 400 °C-annealed dies was ≈ 1.4 at ≈ 0.4 V. The ideality factor for the 700 °C-annealed die was ≈ 1.2 at the same bias voltage. The parasitic resistance of this die was found to be $\approx 60 \Omega$ from the slope of I - V characteristics at 1.5 V, which was close to the sheet resistance of the base layer (~ 1.5 k Ω determined by TLM measurements) divided by 8π , or the estimation of spreading resistance in diodes with circular contacts.²⁸⁾

The difference in the three I - V characteristics of emitter/base diodes implies that the properties of SiC/Si interfaces were improved by the postprocess annealing, which was assumed to cause the increase in the current gain of HBTs. It is noteworthy that the electrical properties of interfaces were improved by annealing at temperatures lower than the highest temperature during the device fabrication process (700 °C)

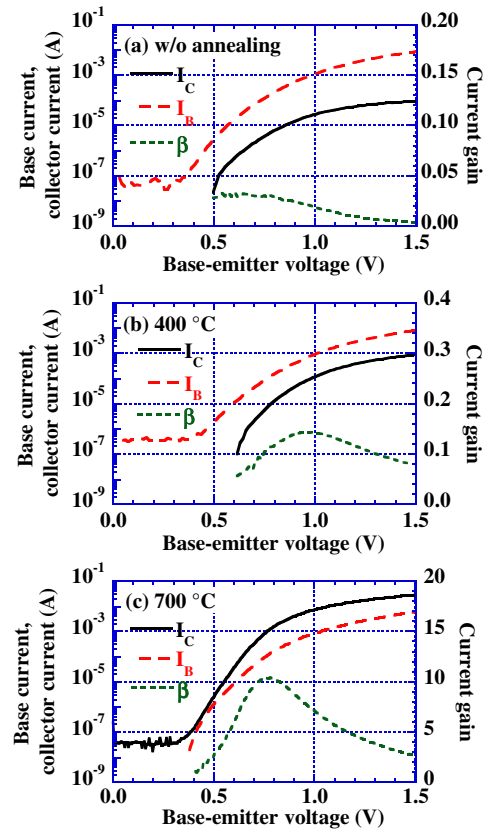


Fig. 6. (Color online) Dependences of I_B , I_C , and β on V_{BE} in 4H-SiC/Si HBT dies without annealing (a), annealed at 400 °C for 1 min (b), and annealed at 700 °C for 1 min (c). V_{CB} was fixed to 0 V.

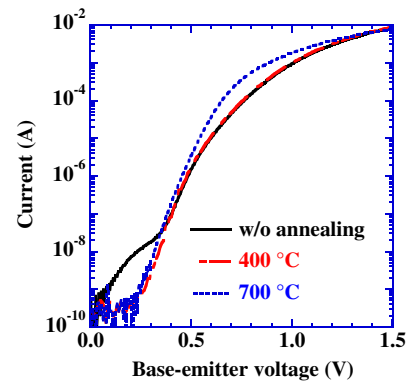


Fig. 7. (Color online) I - V characteristics for forward-bias voltages of nonannealed, 400 °C-, and 700 °C-annealed 4H-SiC/Si emitter/base diodes.

and the reported eutectic point of SiC/Si systems (1410 °C),²⁹⁾ which suggests that the SiC/Si interfaces were in metastable states when the device process was completed. This view is consistent with frequently reported features in SAB-based interfaces that the thicknesses of amorphous layers formed at interfaces immediately after bonding are reduced upon annealing at temperatures lower than the eutectic points.^{18,30)}

Irrespective of the mechanism underlying the enhanced current gain, the obtained β suggests that the intrinsic quality of SiC/Si bonding interfaces is favorable for the minority carriers to be injected across the interfaces with high efficiency at room temperature. HBTs with further improved device performances are likely to be achieved by optimizing the device structures and device fabrication process. The

obtained results, consequently, suggest that SAB is practically useful for fabricating emitter/base junctions, which are vital parts of HBTs.

4. Conclusions

We investigated the transport properties of optically excited and electrically injected minority electrons across SAB-based 4H-SiC/Si interfaces by measuring the photoresponse of pn diodes and the electrical characteristics of HBTs. The threshold energy of the photoresponse spectra of p-Si/n-4H-SiC junctions was close to the bandgap of Si. The increase in photoyield due to reverse-bias voltages was not affected by the energy of incident photons. These findings suggest that optically excited electrons in Si were driven to SiC via tunneling across the potential barrier formed at the interfaces after their energy was relaxed. The current gain in SiC/Si HBTs increased as a result of the postprocess annealing. The maximum common-emitter current gain of >10 was obtained. The increase in the current gain was attributed to the improvement in the electrical properties of the SiC/Si emitter-base interfaces. This means that the SAB-based interfaces are in metastable states and potentially useful as vital parts of semiconductor devices.

Acknowledgment

This work was partly supported by the “Creative Research for Clean Energy Generation Using Solar Energy” project of the Core Research for Evolutional Science and Technology (CREST) program of the Japan Science and Technology Agency (JST).

- 1) T. Ishibashi, *IEEE Trans. Electron Devices* **48**, 2595 (2001).
- 2) H. Matsuzaki, T. Maruyama, T. Kosugi, H. Takahashi, M. Tokumitsu, and T. Enoki, *IEEE Trans. Electron Devices* **54**, 378 (2007).
- 3) A. Elasser and T. P. Chow, *Proc. IEEE* **90**, 969 (2002).
- 4) U. K. Mishra, L. Shen, T. E. Kazior, and Y.-F. Wu, *Proc. IEEE* **96**, 287 (2008).
- 5) O. Moutanabbir and U. Gösele, *Annu. Rev. Mater. Res.* **40**, 469 (2010).
- 6) T. Sugii, T. Yamazaki, and T. Ito, *IEEE Trans. Electron Devices* **37**, 2331 (1990).
- 7) A. Pérez-Tomás, M. R. Jennings, M. Davis, J. A. Covington, P. A. Mawby, V. Shah, and T. Grasby, *J. Appl. Phys.* **102**, 014505 (2007).
- 8) J. Möreke, M. J. Uren, S. V. Novikov, C. T. Foxon, S. H. Vajargah, D. J. Wallis, C. J. Humphreys, S. J. Haigh, A. Al-Khalidi, E. Wasige, I. Thayne, and M. Kuball, *J. Appl. Phys.* **116**, 014502 (2014).
- 9) M. M. R. Howlader, M. J. Deen, and T. Suga, *Jpn. J. Appl. Phys.* **54**, 030201 (2015).
- 10) H. Takagi, K. Kikuchi, R. Maeda, T. R. Chung, and T. Suga, *Appl. Phys. Lett.* **68**, 2222 (1996).
- 11) C. Lian, H. Xing, C. S. Wang, L. McCarthy, and D. Brown, *IEEE Electron Device Lett.* **28**, 8 (2007).
- 12) E. Higurashi, K. Okumura, K. Nakasuji, and T. Suga, *Jpn. J. Appl. Phys.* **54**, 030207 (2015).
- 13) J. Liang, S. Shimizu, M. Arai, and N. Shigekawa, *ECS Trans.* **75** [9], 221 (2016).
- 14) A. Pérez-Tomás, A. Pérez-Tomás, O. J. Guy, R. Hammond, S. E. Burrows, P. M. Gammon, M. Lodzinski, J. A. Covington, and P. A. Mawby, *Electrochem. Solid-State Lett.* **11**, H306 (2008).
- 15) H. Shinohara, H. Kinoshita, and M. Yoshimoto, *Appl. Phys. Lett.* **93**, 122110 (2008).
- 16) A. Pérez-Tomás, M. Lodzinski, O. J. Guy, M. R. Jennings, M. Placidi, J. Llobet, P. M. Gammon, M. C. Davis, J. A. Covington, S. E. Burrows, and P. A. Mawby, *Appl. Phys. Lett.* **94**, 103510 (2009).
- 17) F. Mu, K. Iguchi, H. Nakazawa, Y. Takahashi, M. Fujino, and T. Suga, *Jpn. J. Appl. Phys.* **55**, 04EC09 (2016).
- 18) J. Liang, S. Nishida, M. Arai, and N. Shigekawa, *Appl. Phys. Lett.* **104**, 161604 (2014).
- 19) J. Liang, S. Nishida, M. Arai, and N. Shigekawa, *J. Appl. Phys.* **120**, 034504 (2016).
- 20) T. Okumura and K. Shiojima, *Jpn. J. Appl. Phys.* **28**, L1108 (1989).
- 21) M. Shingo, J. Liang, N. Shigekawa, M. Arai, and K. Shiojima, *Jpn. J. Appl. Phys.* **55**, 04ER15 (2016).
- 22) N. Shigekawa, S. Shimizu, J. Liang, M. Shingo, K. Shiojima, and M. Arai, *Ext. Abstr. 5th Int. Workshop Low Temperature Bonding for 3D Integration*, 2017, p. 26.
- 23) J. Liang, S. Shimizu, S. Nishida, N. Shigekawa, and M. Arai, *ECS Solid State Lett.* **4**, Q55 (2015).
- 24) P. E. Schmid, *Phys. Rev. B* **23**, 5531 (1981).
- 25) S. M. Sze and K. K. Ng, *Physics of Semiconductor Devices* (Wiley, Hoboken, NJ, 2007) 3rd ed., p. 62.
- 26) Y. Taur and T. H. Ning, *Fundamentals of Modern VLSI Devices* (Cambridge University Press, Cambridge, U.K., 2009) 2nd ed., p. 62.
- 27) W. C. Dash and R. Newman, *Phys. Rev.* **99**, 1151 (1955).
- 28) R. L. Pritchard, *Proc. IRE* **46**, 1152 (1958).
- 29) Suherlan, Y.-G. Kim, W. Joung, and I. Yang, *Metrologia* **52**, 330 (2015).
- 30) T. Yu, M. R. Howlader, F. Zhang, and M. Bakr, *ECS Trans.* **35** [2], 3 (2011).